Marine Environmental Research 162 (2020) 105184

Contents lists available at ScienceDirect

Marine Environmental Research

journal homepage: www.elsevier.com/locate/marenvrev

Simulating crude oil exposure, uptake and effects in North Atlantic *Calanus finmarchicus* populations

Ole Jacob Broch [a,*], Raymond Nepstad [a], Ingrid Ellingsen [a], Radovan Bast [b], Geir Morten Skeie [c], JoLynn Carroll [c]

[a] SINTEF Ocean, Postboks 4762 Torgarden, 7465 Trondheim, Norway
[b] High Performance Computing Group, IT Department, UiT The Arctic University of Norway, 9037 Tromsø, Norway
[c] Akvaplan-niva, FRAM – High North Research Centre for Climate and the Environment, 9296 Tromsø, Norway

ABSTRACT

A simulation model framework (SYMBIOSES) that includes a 3-dimensional ocean physics and biology model and a model for transport and fate of oil was used to investigate the potential for bioaccumulation and lethal/sublethal effects of oil components in the copepod *Calanus finmarchicus* in the Lofoten–Vesterålen archipelago of Norway. The oil model is coupled with the biology model by way of a bioaccumulation model, from which mortality and reduction in reproduction are calculated via a total body burden (TBB). The simulation results indicate that copepod body burden levels are affected by the spill type (surface spill, subsea blowout) and the spill timing (spring, autumn). The effects of oil component bioaccumulation on the copepod population for all scenarios are small, though greatest in the subsea blowout scenarios. We attribute this to the limited spatial and temporal overlap between copepods and oil in the environment simulated by the model. The coupling of the processes of oil transport, bioaccumulation/excretion and the associated effects are discussed in the context of the model framework and with a view towards applications for Ecological Risk Assessment (ERA).

1. Introduction

Copepods are a ubiquitous and integral part of marine ecosystems and food webs. In the North Atlantic, the zooplankton copepod *Calanus finmarchicus* is important both as a food source for higher trophic levels (Helaouët and Beaugrand, 2009) and as part of cycling and vertical transport of carbon in the ocean through seasonal vertical migration (Jónasdóttir et al., 2015). Any large-scale anthropogenic perturbation of the *C. finmarchicus* population may pose a risk to the stability of the marine ecosystem. Relevant stressors include harvesting of *Calanus spp*, climate change with implications for ocean warming and acidification, and potentially also marine oil spills.

The Norwegian shelf region off the Lofoten–Vesterålen archipelago (LoVe) (Fig. 1, archipelago within the yellow box) is an important breeding ground for Northeast Arctic cod, whose larval stages depend on *C. finmarchicus* nauplii for food (Misund and Olsen, 2013). This region is further of great importance for the entire production in the Arctic Ocean (AO) because a significant part of the primary and secondary production necessary to sustain the AO ecosystem is advected past LoVe and into the Barents Sea and AO (Wassmann et al., 2019; Vernet et al., 2019).

C. finmarchicus has a life cycle of six naupli (NI to NVI) and six copepodite (CI to CVI) stages. Overwintering copepodites, mainly stage CV (Conover, 1988), overwinter in deep trenches, fjords and off the shelf. They begin an upward migration to the sea surface in late winter, molt into adults (CVI) and subsequently spawn. The rates of *C. finmarchicus* development depend on temperatures and food availability. In the LoVe region the new CV stages start their descent for diapause in early summer (Melle et al., 2014). The *C. finmarchicus* biomass varies significantly from one year to another (Alver et al., 2016; Weidberg and Basedow, 2019), and the population is heterogeneously distributed on the LoVe shelf (Slagstad and Tande, 2007; Weidberg and Basedow, 2019).

The distribution of the *C. finmarchicus* population results from the interactions between diurnal and seasonal migration patterns and a complex oceanographic system (Fig. 2). Two major ocean current systems enter LoVe from the south: The Norwegian Coastal Current (NCC), driven by brackish outflow from the Baltic and freshwater runoff along the Norwegian coast, and the North Atlantic Current (NAC). The NCC splits into two branches at around 67° N, one following the 200–300 m depth contours (Sætre, 2007), the other one flowing along the coast, continuing southwards along the northern side of the Vestfjord (Mitchelson-Jacob and Sundby, 2001). The branches meet again outside the westernmost island group in the Lofoten archipelago. Tidal currents push water back and forth through channels separating the Lofoten islands, creating eddies and generating internal waves. Outside Lofoten there are several bank regions and canyons along the slope that further influence local circulation patterns. The narrowing of the shelf

* Corresponding author.
E-mail address: ole.jacob.broch@sintef.no (O.J. Broch).

https://doi.org/10.1016/j.marenvres.2020.105184
Received 5 May 2020; Received in revised form 30 September 2020; Accepted 6 October 2020
Available online 8 October 2020

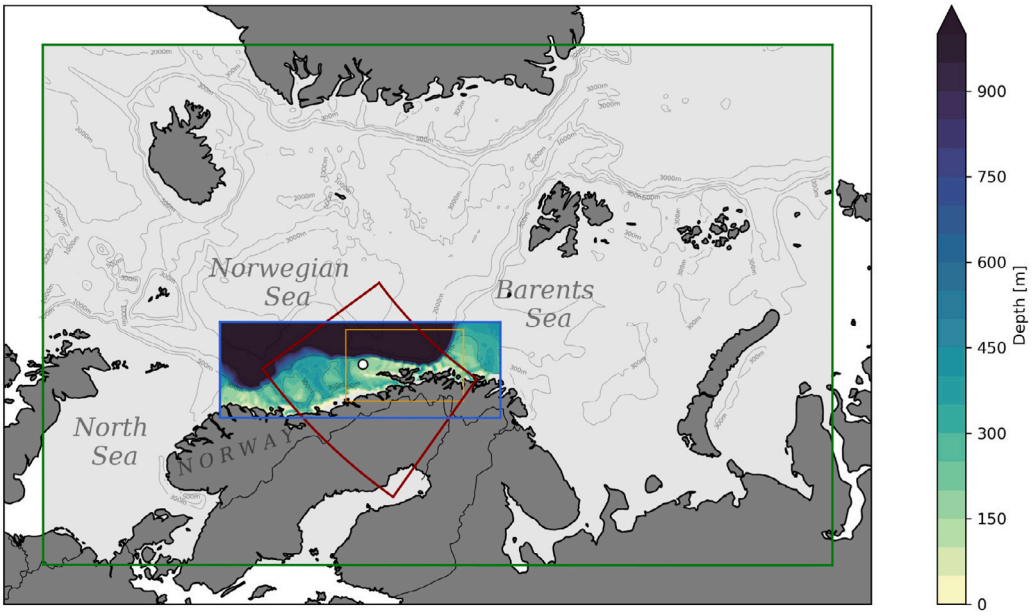

Fig. 1. SINMOD and OSCAR model domains used in the simulation scenarios are outlined in blue and red, respectively. The colors within the blue rectangle indicate bathymetry. The larger rectangle with a green boundary indicates the larger 4 km model domain that generated boundary conditions for the blue model domain. The discharge point (67.7° N, 10.84° E) is indicated by a white dot. The yellow box indicates the seas around the Lofoten–Vesterålen (LoVe) region. (For interpretation of the references to color in this figure legend, the reader is referred to the web version of this article.)

outside Vesterålen results in high current speeds in the NCC and the NAC, leading to frontal instabilities. Eddies formed in the area transport pockets of coastal water out into the Lofoten basin (Gascard et al., 2004; Isachsen, 2015).

In the present paper we study the interactions between dispersal of dissolved oil and the copepod *Calanus finmarchicus* using the ecosystem effects model framework SYMBIOSES (Carroll et al., 2018). The framework couples physics, biology, oil dispersal, bioaccumulation and effects models. Processes such as oil uptake and retention, transport, and the overlap of oil and *C. finmarchicus* in space and time (match–mismatch) are considered. Different oil spill scenarios were run for a single location on the shelf in order to contrast surface and sea bed (blowout) releases in spring and autumn.

The key questions that we address are:

- What is the relationship between the type of discharge and the bioaccumulation of oil components in the population of *C. finmarchicus*?
- What is the relationship between the timing of oil release and bioaccumulation?
- How do these factors relate to the acute lethal and sub-lethal effects of oil components bioaccumulated in copepods?

The results from the simulations are discussed in the context of the processes resolved by the model system. They are further discussed with a view towards the use of spatially resolved simulation results in ecological risk assessment tools.

2. Materials and methods

2.1. SYMBIOSES model framework

The SYMBIOSES model framework is described in Carroll et al. (2018) (and references therein). It contains several model components: a 3D coupled hydrodynamics and lower trophic levels model system (SINMOD) including a stage structured population model for the copepod *Calanus finmarchicus*; the oil transport and fate model OSCAR; an individual-based model (IBM) for cod larvae; and a forward-simulation model of fish population dynamics (Globally applicable Area-Disaggregated General Ecosystem Toolbox (GADGET)) to simulate cod adults and juveniles from age 1 year (Howell and Bogstad, 2010).

2.1.1. Hydrodynamics–ecosystem model

SINMOD is a coupled 3D hydrodynamic biogeochemical model system (Slagstad and McClimans, 2005; Wassmann et al., 2006) of the North Atlantic and Arctic Oceans (Lee et al., 2016). The hydrodynamic model component uses *z*-layers, *i.e.* all but the top and bottom vertical layers have fixed thicknesses. A hydrostatic approximation is applied (the pressure at a given depth equals the sum of the atmospheric pressure and the weight of the water above). The food-web model for the lower trophic levels includes states for nutrients, the bacterial loop, phytoplankton, ciliates and zooplankton, represented here by *Calanus finmarchicus*.

The 4 km resolution model domain used in the present study was nested (receiving boundary conditions) from a larger 4 km model (Fig. 1), in turn nested from a 20 km model domain, covering the Norwegian Sea, the Barents Sea and the Arctic (Alver et al., 2016). The depth layers used ranged from 10 m near the surface to 500 m at greater depths. Bathymetry data for the model was provided by the Norwegian Mapping Authority (www.kartverket.no) with additional data from the International Bathymetric Chart of the Arctic Ocean (www.ibcao.org). The 20 km model was forced with tidal components M_2, S_2, K_1, and N_2 at the open boundaries with data on global ocean tides imported from the TPXO 6.2 model (http://www.coas.orgeonstate.edu/research/po/research/tide/global.html). Atmospheric forcing was applied using ERA-Interim data from the European Centre for Medium-Range Weather Forecasts (ECMWF) (Dee et al., 2011). Freshwater runoff from rivers and land was supplied by the Norwegian Water Resources and Energy Directorate (www.nve.no). The simulation time step was 360 s according to standard numerical stability criteria. The larger 4 km model from which the present model simulations were nested, was subject to a spin up period of ~20 years prior to the simulation start. The model has been shown to resolve the circulation dynamics at the Norwegian Shelf off Northern Norway (Slagstad et al., 1999; Skardhamar and Svendsen, 2005; Anon, 2011).

2.1.2. Oil dispersal and fate model

The OSCAR model simulates transport and fate of the oil spilled, based on a Lagrangian particle formulation (Reed et al., 2004; Pan et al., 2020). Oil is represented using 25 pseudocomponent groups

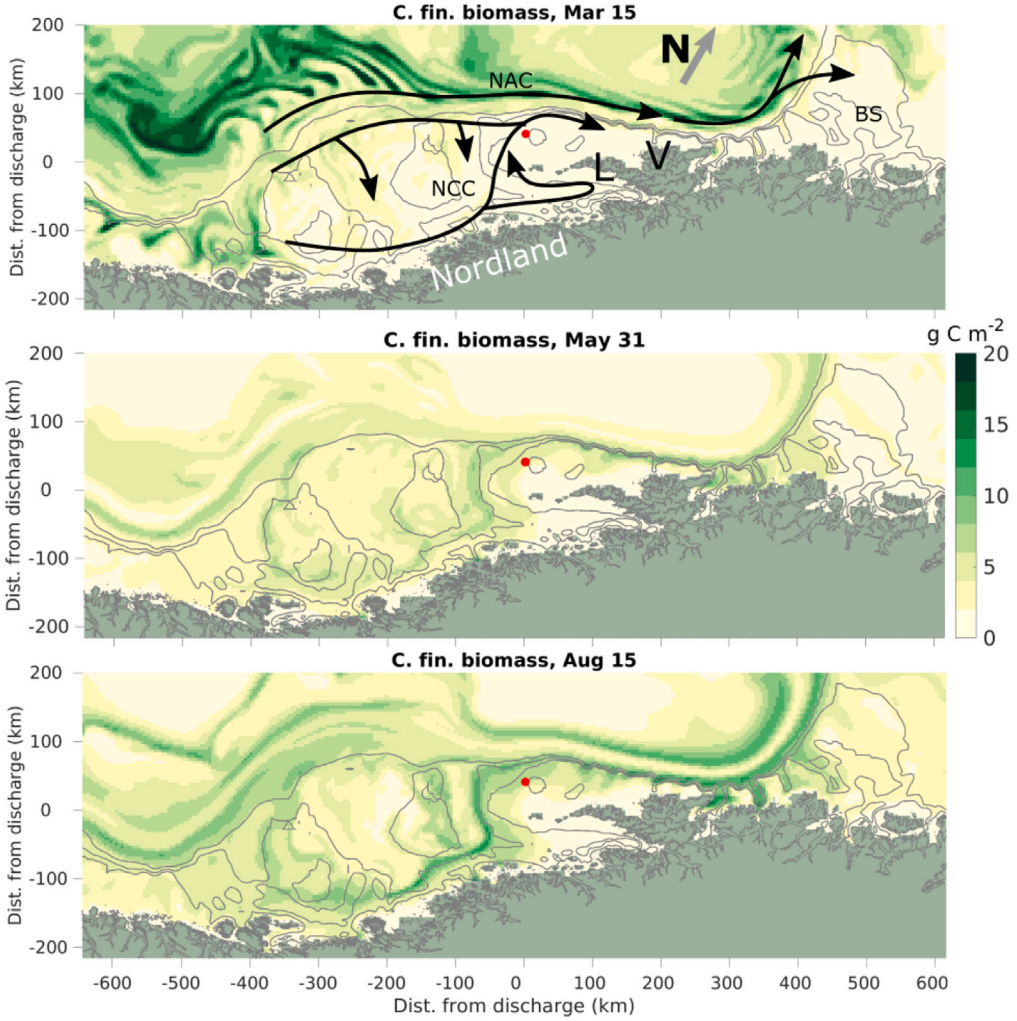

Fig. 2. Depth integrated (entire water column) simulated biomass of *C. finmarchicus* in the baseline scenario (no oil effects) on March 15 (top), May 31 (middle), and August 15 (bottom). The gray curves indicate 200, 300, and 500 m isobaths. The coastline of part of Nordland county is indicated, as are the Lofoten (L) and Vesterålen (V) archipelagos. The main flows of the Norwegian Coastal Current (NCC) and the North Atlantic Current (NAC) are indicated. They are transport pathways into the Arctic, splitting up into a Northern and an Eastern branch into the Barents Sea (BS). The red dot indicates the discharge point used in the oil dispersal scenarios (Table 2).

with different chemical properties, and is tracked across surface slick, droplet and dissolved phases. Oil droplets tend to have lower bulk density than the surrounding water, and will rise to the surface with a speed determined by their relative density and diameter, see Eq. 4 in Rye et al. (2008), while also undergoing transport with the prevailing currents. Dissolved oil is transported as a tracer, while surface oil also experiences wind drag, in addition to breakup by wind-wave action, resulting in entrained oil droplets. Subsea blowouts generate a plume which is modeled by an integrated multiphase plume model, accounting for bulk buoyancy and effects of entrainment (see Johansen (2000) for details).

The pseudocomponent approach assumes that individual hydrocarbon constituents in a given group behave similarly (i.e., have similar distributions and fates in the environment). Each Lagrangian oil particle contains a time-dependent amount of each pseudocomponent, and these are transported together. Weathering processes operate on individual pseudocomponents and include surface evaporation, biodegradation and emulsification. Generally, the lighter components (e.g. Benzene) evaporate, dissolve and biodegrade faster than the heavier components (e.g. PAHs). More details of the pseudocomponent properties are given in Reed et al. (2000), Pan et al. (2020). Current and wind forcing fields are input to OSCAR, and are provided by the hydrodynamic model through the SYMBIOSES model coupling interface (Carroll et al., 2018).

OSCAR uses a geographical coordinate system, which is different from the polar stereographic grid used by the circulation model. In the present simulation, OSCAR has been set up in a 1.3 km horizontal resolution using 30 m vertical layers between 0 and 300 m water depth (red region in Fig. 1). The grid is used to reconstruct the concentration fields for each pseudocomponent, in turn used by the exposure and effect models.

2.1.3. *Calanus finmarchicus* model

The *C. finmarchicus* model is a stage structured dynamical population model. The version used here has 29 mathematical compartments for the physiological CI–CVI stages (Fig. 4). The physiological stage CVI (females) is further subdivided into 12 mathematical stages. Thus, the total number of mathematical compartments for the copepodite stages used here is 40. In addition there is an egg compartment and 8 mathematical compartments for the nauplii stages NI–NVI. The model, coupled with the basic food web model, has previously been applied to studying the dispersal and direct toxic effects of produced water in the Lofoten–Vesterålen region (Broch et al., 2013), though without inclusion of a model for oil fate, bioaccumulation and effects.

The individual carbon content ($\mu g\, C\, individual^{-1}$) for each mathematical level follows an exponential law:

$$C(j) = e^{b_C(j-1)},\ j = 1, \ldots, 28;\ C(29) = 131; \quad (1)$$

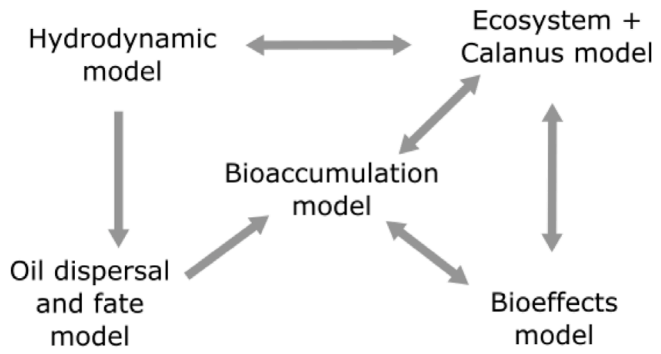

$$\frac{\partial C}{\partial t} + g_w \frac{\partial C}{\partial w} + \sum_{i=1}^{25} (a_i - b_i) \frac{\partial C}{\partial B_i} + \mathcal{A}(C) + \mathcal{D}(C) = \text{Birth} - \text{Mortality}.$$

Fig. 3. The main model components and how they interact with one another. The main equation connects some of the main processes to the stage-distributed *C. finmarchicus* biomass C through advection and diffusion, growth, bioaccumulation and excretion, and mortality. Here the terms "Birth" and "Mortality" include the added effects from the bioaccumulated oil components. The body burden of component number i is denoted by B_i, while accumulation and excretion of each body burden is denoted by a_i and b_i, respectively. See Table 1 for the definition of all variables and parameters used. The absorption and attenuation with depth of the shortwave radiation depends on the chlorophyll concentration. This affects the water temperature, so that there is two-way coupling between the ecosystem/lower trophics and the physics modules.

(Alver et al., 2016; Carlotti et al., 1993); Fig. 4. The value of b_C is recorded in Table 1. Growth rates are calculated from food availability (ciliates and diatoms, c.f. Wassmann et al. (2006)) and temperature. The non-diapausing copepod levels for *C. finmarchicus* are assumed to be distributed in the depth range from 10 to 50 m (Conover, 1988). The overwintering population (CV stages) is assumed to be normally distributed with a mean depth of 800 m ($\sigma = 300$), limited of course by the bottom depth and the surface at the pertinent location.

Ascent from diapause is assumed to start on January 1 and continue gradually until April 1. Most of the copepods completing the CV stage before August 1 are assumed to enter the overwintering population and start the descent, while the remaining copepods continue development and may contribute to a second spawning cycle. After August 1, all copepods completing the CV stage are assumed to enter the overwintering population.

The details of the model, including all parameters for developmental-, feeding-, and spawning rates, are provided in Slagstad (1981) and Alver et al. (2016). In Alver et al. (2016) a partial validation, in particular for stages CII and CIII, is also made.

2.1.4. Bioaccumulation and effects models

Bioaccumulation of oil components in the *C. finmarchicus* module is handled by the Optimal Modeling for Ecotoxicological Assessment (OMEGA) model implemented following Hendriks et al. (2001) and described in DeHoop et al. (2016). Dilution of the body burdens (BBs) is handled by the growth calculation in the *C. finmarchicus* model and there is no transfer of oil components from phytoplankton to *C. finmarchicus*. There is one internal BB for each of the 25 OSCAR pseudocomponents (Section 2.1.2), denoted $B_i, i = 1, \ldots, 25$, for each mathematical *C. finmarchicus* level. Thus, there are individual uptake and retention dynamics for each of the 40 × 25 BBs, depending on the octanol–water partition coefficient (Kow) for the specific components and the lipid content of the mathematical *Calanus* levels, in addition to the internal and external concentrations and the wet weight of the animals (Hendriks et al., 2001).

A fixed lipid content (unit: µg) for each mathematical *C. finmarchicus* level has been introduced, following the equation:

$$L(j) = a_L e^{b_L j},\ j = 1, \ldots, 28;\ L(29) = 65.5, \tag{2}$$

where again $j = 29$ represents the 12 CVI stages. The values of the parameters a_L and b_L, are recorded in Table 1. We assume the wet weight W, used in the bioaccumulation model (OMEGA) to be

$$W(j) = 10C(j),\ j = 1, \ldots, 29. \tag{3}$$

This is similar to the relation used in Coyle and Gibson (2017).

Increased mortality m and the reproduction fraction r due to the level of the total body burden are calculated from the Total Lipid Specific Body Burden (TBB_{lip}) following DeLaender et al. (2011) as follows:

$$m(TBB_{\text{lip}}) = \log\left(1 + \left(\frac{TBB_{\text{lip}}}{LBB}\right)^{\gamma}\right) T_{exp}^{-1}, \tag{4}$$

and

$$r(TBB_{\text{lip}}) = \left(1 + \left(qls\frac{TBB_{\text{lip}}}{LBB}\right)^{\gamma}\right)^{-1} \tag{5}$$

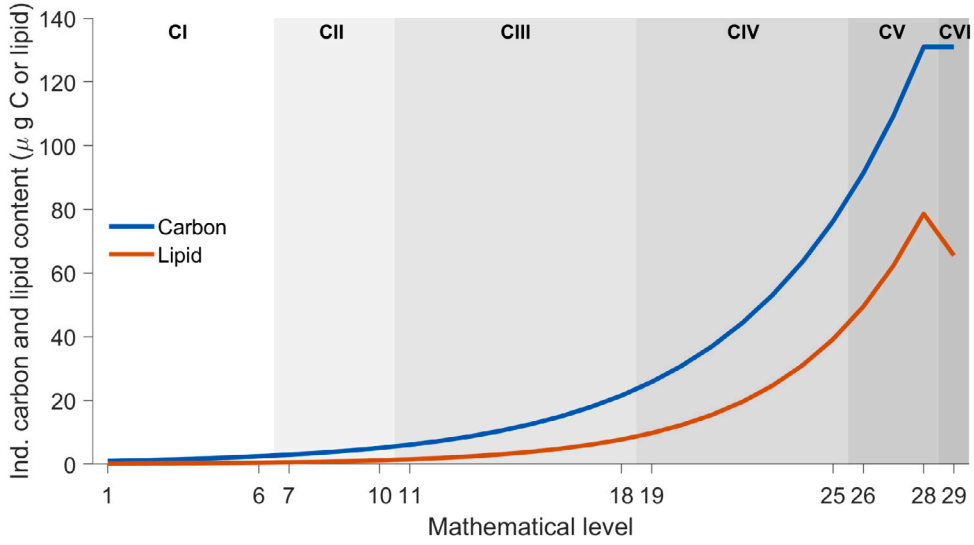

Fig. 4. Relationships between mathematical compartments (1 to 29), individual weights (µg C, blue curve; equation (1)) and physiological stages (CI to CVI, indicated by different shades of gray) in the *C. finmarchicus* model. The fixed lipid content of each mathematical level is also indicated (orange curve (µg lipid), Eq. (2)). The parameters for the curves are recorded in Table 1. (For interpretation of the references to color in this figure legend, the reader is referred to the web version of this article.)

Table 1
List and explanation of the main abbreviations, notation, variables and parameters used. The numerical values of certain parameters are included where relevant.

Model or subject	Symbol/ concept	Definition	Numerical value and/or unit	References and remarks
Ocean-ecosystem-Calanus model	A_j	Abundance of *C. finmarchicus* mathematical compartment number j	ind m^{-2}	Alver et al. (2016)
	C	*C. finmarchicus* individual carbon content	$\mu g\, C\, ind^{-1}$	Alver et al. (2016)
	b_C	*C. finmarchicus* stage-carbon relation parameter in Eq. (1)	0.1806 $stage^{-1}$	Alver et al. (2016)
	L	*C. finmarchicus* individual lipid content	μg lipid ind^{-1}	This paper
	W	*C. finmarchicus* individual wet weight	$\mu g\, ind^{-1}$	This paper
	a_L	*C. finmarchicus* stage-lipid content relation parameter in Eq. (2)	0.119 μg lipid ind^{-1}	This paper
	b_L	*C. finmarchicus* stage-lipid content relation parameter in eq (2)	0.2319 $stage^{-1}$	This paper
	$\mathcal{A}$	Advection operator		Wassmann et al. (2006)
	D	Diffusion operator		Wassmann et al. (2006)
Bioaccumulation and effects model	m	Added mortality due to toxicity	day^{-1}	DeLaender et al. (2011) and DeHoop et al. (2016)
	r	Reproduction fraction due to toxicity	Dimensionless	DeLaender et al. (2011) and DeHoop et al. (2016)
	LBB	Lethal body burden	83.76 mmol (kg lipid)$^{-1}$	DeLaender et al. (2011) and DeHoop et al. (2016)
	TBB	Total body burden	mmol (kg lipid)$^{-1}$	DeLaender et al. (2011) and DeHoop et al. (2016)
	γ	Slope of effects curve	5.36	DeLaender et al. (2011) and DeHoop et al. (2016)
	q_{ls}	Lethal–sublethal ratio	1.14	DeLaender et al. (2011) and DeHoop et al. (2016)
	T_{exp}	Experimental exposure time	10 days	DeLaender et al. (2011) and DeHoop et al. (2016)

The TBB_{lip} is calculated following DeHoop et al. (2016) and has the unit of mmol (kg lipid)$^{-1}$ in this context. Thus, the effect of the bioaccumulated oil components is to reduce the reproduction rate (number of eggs laid per unit time; Alver et al. (2016)) by a fraction $1 - r$. The mortality rates were added to the basic mortality rates, e.g. those applied when there are no effects of accumulated oil components. The basic mortality rates lie in the range 0.025 to 0.055 d^{-1} for the CI to CV stages and in the range 0.013 to 0.039 d^{-1} for the adult females (Slagstad and Tande, 2007; Alver et al., 2016). The mortality for the overwintering CV animals is generally low, but is increased for animals residing in shallow waters (Alver et al., 2016). The parameter values used in the lethal and sub lethal effects Eqs. (4), (5) are recorded in Table 1 and are based on average species sensitivity (DeHoop et al., 2016).

For comparison between external an internal concentrations of the oil components, we use the wet weight specific body burden for copepodite stages $l \in \{\mathrm{I}, \mathrm{II}, \mathrm{III}, \mathrm{IV}, \mathrm{V}, \mathrm{VI}\}$ ($TBB_{w,l}$) given for each horizontal location (x, y) by:

$$TBB_{w,l}(x,y) = \frac{\sum_{i=1}^{25} \sum_{j=l_{low}}^{l_{up}} B_{j,i}(x,y) W(j) A_j(x,y)}{\sum_{j=l_{low}}^{l_{up}} W(j) A_j(x,y)}, \tag{6}$$

with unit $\mu g\ kg^{-1}$. Here l_{low} and l_{up} denote the lower and upper mathematical indices of physiological stage l (Fig. 4). $A_j(x, y)$ denotes the depth integrated abundance (ind m^{-2}) of mathematical compartment j in horizontal position (x, y). We also calculate a total body burden for all the stages in a position (x, y) combined:

$$TBB_{w}(x,y) = \frac{\sum_{i=1}^{25} \sum_{j=1}^{29} B_{j,i}(x,y) W(j) A_j(x,y)}{\sum_{j=1}^{29} W(j) A_j(x,y)}. \tag{7}$$

Finally, we calculate a Total Population Body Burden TBB_{pop} for a spatial region Ω, as the total concentration of dissolved pseudo components in the entire population:

$$TBB_{pop}(\Omega) = \frac{\int_{\Omega} \left(\sum_{i=1}^{25} \sum_{j=1}^{29} B_{j,i}(x,y) W(j) A_j(x,y) \right) dm}{\int_{\Omega} \left(\sum_{j=1}^{29} W(j) A_j(x,y) \right) dm}. \tag{8}$$

We similarly compute area-averages for each physiological stage.

The growth dynamics, absorption and elimination of BBs, birth and mortality and physical advection are all linked through the equation presented in Fig. 3. See also (DeHoop et al., 2016).

2.2. Simulations and oil release scenarios

The simulation scenarios described here were started on March 1 and August 1, 1995. These start times represent the beginning of the spring bloom and late in the summer when biological production is waning. The hydrodynamic and ecosystem modules were started from pre-computed initial fields from simulations that had been run over ~20 years' simulated time. While there may be significant local and short-term variation in the ocean currents in the region studied here, due to wind patterns, stratification, and topographic influences, the direction of the two main current systems, NAC and NCC, remain the same (Skardhamar and Svendsen, 2005). The four oil release scenarios include both surface spills and subsea blowouts (Table 2). In addition a baseline scenario without any oil release was run. An oil release was initiated at the start of the simulation and lasted for 90 days in all cases. The total simulation time was 180 days. A release duration of 90 days is considered to be a severe oil spill event, comparable to the duration of the Deepwater Horizon (DWH) spill release. However, oil release rates are controlled by reservoir characteristics (Carroll et al., 2018). Based on expert knowledge of our study location, we selected a release rate of approximately half the volume of the DWH oil spill, or 4500 m3/d. This release rate is also the P90% oil spill release rate estimated by the Norwegian Petroleum Directorate for this region, and is thus representative of a "worst case" scenario. The bottom depth at the release point is representative of the depth of the shelf around the LoVe region (200–300 m, Fig. 2).

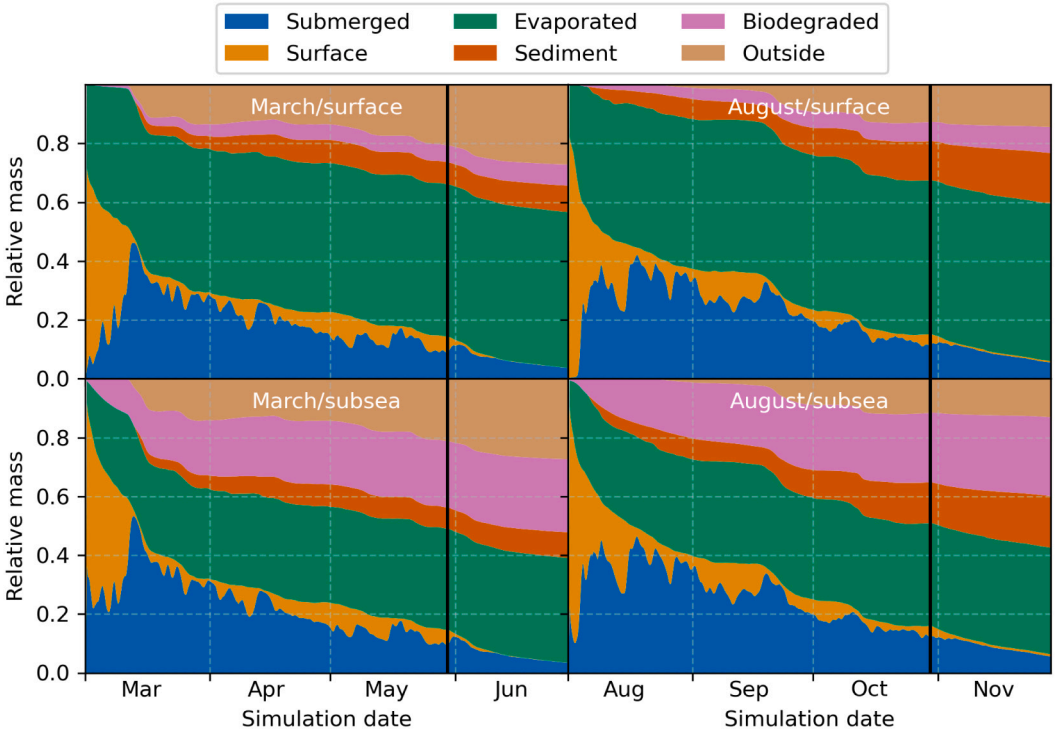

Fig. 5. Global normalized mass balance of oil, showing the total relative mass of oil in a given compartment (see figure legend) over time. The different scenario parameters are described in the text and in Table 2. The vertical, black lines indicate the time when the oil release ended.

Table 2
Summary of the most important features of the oil release scenarios simulated. A subsea blowout is initiated at the sea bed, and generates a positively buoyant plume which rises towards but does not reach the surface. A surface release is at the water surface, initially forming a slick which over time is broken up into droplets and mixed into water column by wind-waves.

	Scenario A	Scenario B	Scenario C	Scenario D
Oil type	Draugen	Draugen	Draugen	Draugen
Release type	*Surface*	*Surface*	*Blowout*	*Blowout*
Release rate (m^3/d)	4500	4500	4500	4500
Release duration (days)	90	90	90	90
Release start	*March*	*August*	*March*	*August*

3. Results

3.1. Baseline *C. finmarchicus* distribution and temporal development

In the baseline scenario without oil release, the simulated distribution of *C. finmarchicus* on the Norwegian shelf followed an expected seasonal pattern. At the beginning of the simulation period (March, Fig. 2, top panel), the highest concentrations of *C. finmarchicus* were found off the continental shelf (bottom depth > 500 m) and on the shelf offshore Central Norway in the southern part of the model domain. The biomass further north at this time occurred due to advection into the region rather than local production (Wassmann et al., 2019). As primary production and temperatures increased further north, so did the local production of *C. finmarchicus*.

Later (May, Fig. 2, middle panel) there was higher biomass of *C. finmarchicus* along the Nordland coast, particularly in a ribbon along the NCC. At this time, there was a relatively high biomass on the shelf further north, and some transport of *C.finmarchicus* both eastward in the direction of the Barents Sea and northward, both routes into the Arctic (Fig. 2). This was more pronounced in August (Fig. 2, bottom panel). By August much of the adult population had entered diapause, descending to greater depths in the trenches along the shelf break off Lofoten and Vesterålen. Note that the biomass concentrations on the shelf were relatively low compared to the concentrations outside the shelf throughout the entire simulation period.

3.2. Oil spill patterns

The Draugen oil type contains a large fraction of lighter oil components, resulting in a high percentage of oil removal by evaporation according to the simulation results, as shown in mass balance Fig. 5. The Draugen scenarios also result in a large fraction of dissolved oil components, particularly for the subsea blowouts. A subsea blowout is initiated at the sea bed (183 m water depth), and generates a positively buoyant plume which rises towards but does not reach the surface; after approximately 10 min it is trapped at 53 m depth, after which the plume phase terminates, and oil is released to the far field where transport and weathering occurs on the oil-containing individual Lagrangian particles. Oil droplets will continue to rise towards the surface with speeds determined by their diameter and relative density. A surface release occurs at the sea surface, initially forming a slick which over time is broken up into droplets and mixed into water column by wind-waves. Between 43–62 percent of discharged oil is lost through the processes of biodegradation and evaporation combined (Fig. 5). Biodegradation removes more oil for subsea discharges compared to surface, while the opposite is true for evaporation. While the simulated dissolved oil component concentrations are similar for comparable surface and subsea scenarios, subsea discharge scenarios exhibit significantly more dissolved oil as well as higher maximum and mean concentrations relative to surface scenarios. The composition of dissolved oil also differs. For surface releases, PAH-type compounds dominate while for subsea releases, light/medium saturates dominate (data not shown). There was greater differences in the horizontal distribution patterns of oil between the March and August simulations than between the surface spill and subsea blowout simulations (Table 2, Fig. 6). This difference was caused by differing current and wind patterns between the two simulation periods. There was some mixing southward in the March simulations but not in the August simulations as seen from the gray regions in Fig. 6.

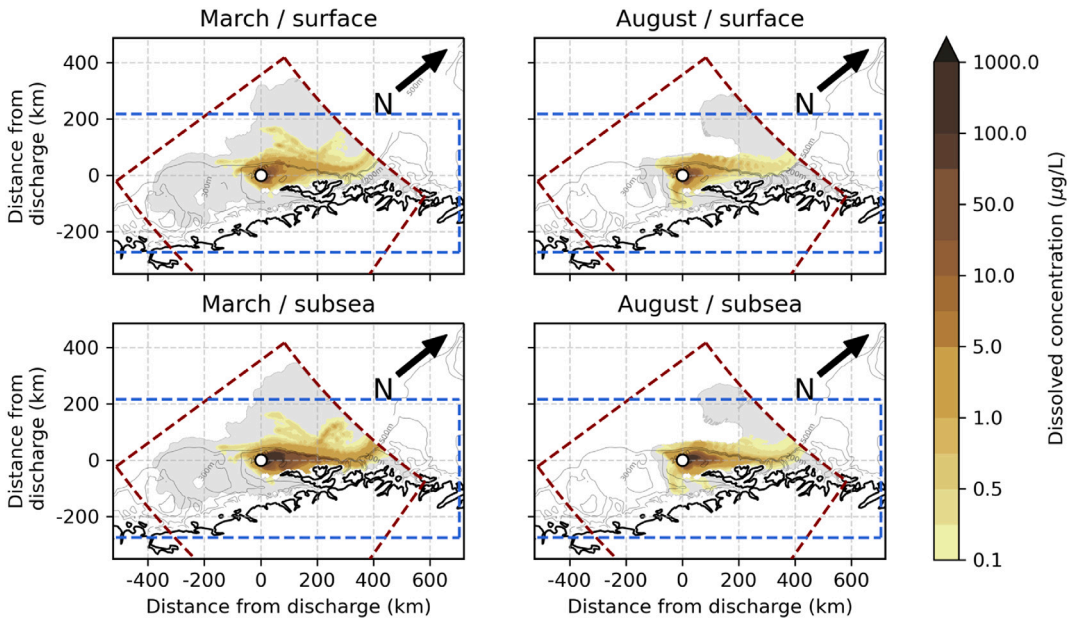

Fig. 6. Dissolved oil concentrations, summed over all pseudocomponents, and with the maximum value taken over the whole oil simulation tracking period (120 days) and depth. A logarithmic color scale is used, showing concentration values from 1–3000 µg L^{-1}; the gray areas indicate where oil may occur during the simulation period, below these concentrations. The outline of the oil spill model grid is shown (dashed red line), as well as the ocean model grid (blue line), while the black-and-white circle indicates the discharge point. The different scenario parameters are described in the text. (For interpretation of the references to color in this figure legend, the reader is referred to the web version of this article.)

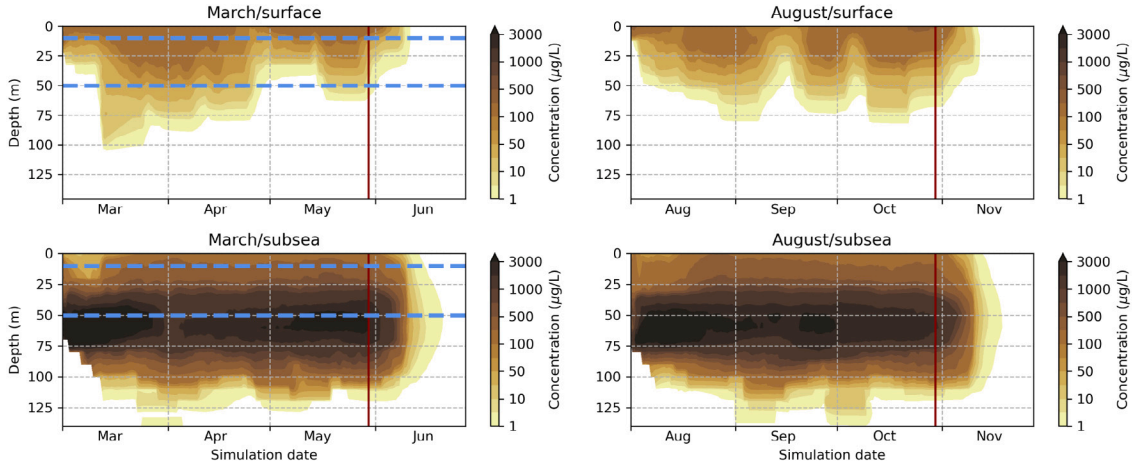

Fig. 7. Horizontal maximum of dissolved oil concentration at different depths and times, summed over all pseudocomponents. Only concentrations > 1 µgL^{-1} are shown. The different scenario parameters are described in the text. The end of the discharge after 90 days is indicated by the vertical red lines. The dashed, blue lines in the left panels (March simulations, scenarios A and C) indicate the depth distribution of the *C. finmarchicus* copepodites during this period. (For interpretation of the references to color in this figure legend, the reader is referred to the web version of this article.)

The vertical profiles of oil concentrations (horizontal maximum) differed more between the surface spill and subsea blowout scenarios than between the March and August scenarios (Fig. 7).

3.3. Bioaccumulation of oil components in C. finmarchicus

The maximum TBB_w over time (all stages combined, Eq. (7)) was spatially distributed in a pattern similar to that for the concentrations of oil pseudocomponents (Figs. 6 and 8). There were differences between all four scenarios (2 release depths, 2 start times) on the one hand, and similarities between the groupings of simulations on the other (March vs. August, surface spill vs. subsea blowout). In the March scenario results (Figs. 8A, C) there was a band of relatively high TBB_w outside the shelf break that was not present in the August scenario results (Figs. 8B, D). In the blowout scenarios (Figs. 8C, D) the regions with the highest TBB_w were larger than in the surface release scenarios (Figs. 8A, B).

The maximum values of the population TBBs (TBB_{pop}, Eq. (8)) over time were similar in the March and August scenarios (Fig. 9), while in the blowout scenarios the maximum TBB_{pop} was almost twice as high as in the surface release scenarios (Fig. 9). The highest values of TBB_{pop} were achieved in the March blowout scenario (Scenario C, Table 2) during the period from late April to early June.

Comparing the TBB and the oil component concentrations by model grid cells (a point-by-point Pearson correlation for the SINMOD domain) (Figs. 6, 8), there was no direct relation between the TBB and the concentrations of oil components. This illustrates the combined effects of bioaccumulation of oil components and advection of the BBs. It hints at the importance of sampling the biota in addition to the water for information on the severity and history of an oil spill.

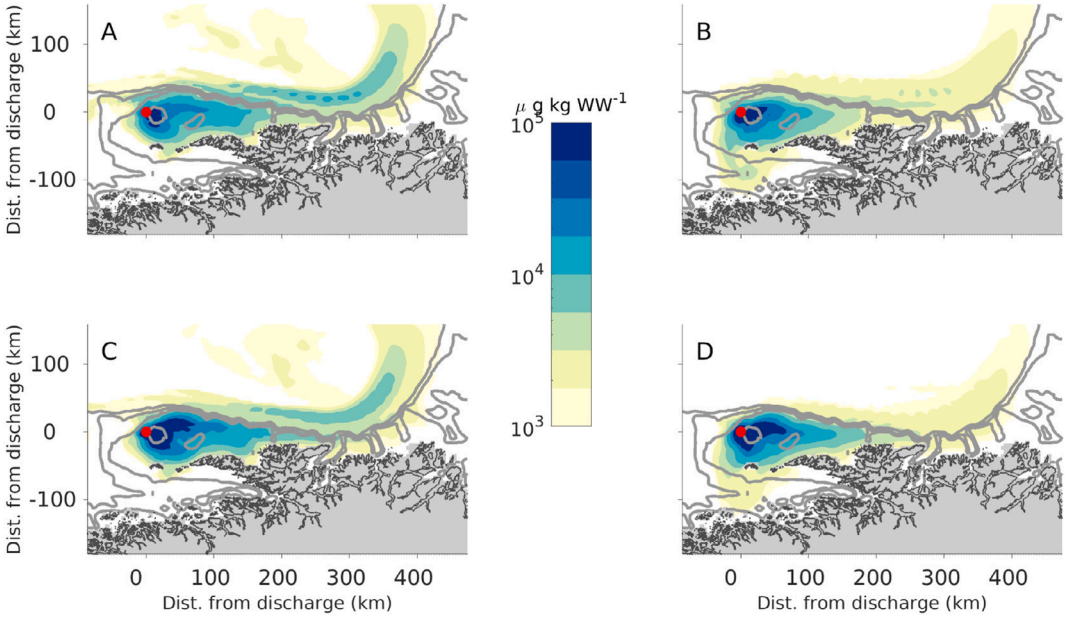

Fig. 8. Spatial plots of the time-maximum TBB_w (over all stages, Eq. (7)) in scenarios A, B, C, and D. The colors indicate the TBB in μg (kg wet weight)$^{-1}$. Note the logarithmic color scale. Only values above 10^3 μg (kg we weight)$^{-1}$ have been plotted. The gray curves indicate the 200, 300, and 500 m isobaths. The region covered is indicated by the yellow rectangle in Fig. 1. The red dot indicates the discharge point used in the oil dispersal scenarios (Table 2). (For interpretation of the references to color in this figure legend, the reader is referred to the web version of this article.)

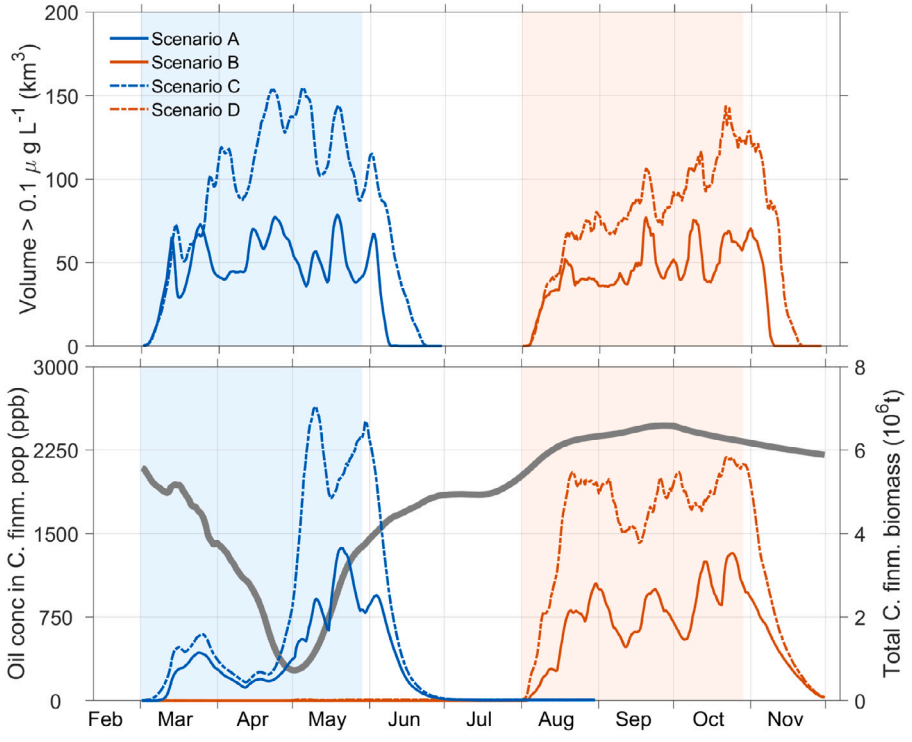

Fig. 9. Top: Volume of water where oil concentration exceeds 0.1 μg L^{-1}, integrated over the top 50 m of the water column (the oil that is available for bioaccumulation in *C. finmarchicus*. Bottom: time series of oil in the total *C. finmarchicus* population for the year 1995 (μ g oil components (kg wet weight)$^{-1}$). The thick, gray curve represents the total simulated depth and stage integrated *C. finmarchicus* biomass within the yellow box in Fig. 1 in the baseline (no oil) scenario. The blue curves represent the March oil release scenarios (A, surface spill and continuous line; C, subsea blowout and dashed line), while the maroon curves represent the August scenarios (B, surface spill and continuous line; D, subsea blowout and dashed line). See Table 2. The light blue (resp. pink) shaded region indicate the period of the March (resp. August) release scenarios. (For interpretation of the references to color in this figure legend, the reader is referred to the web version of this article.)

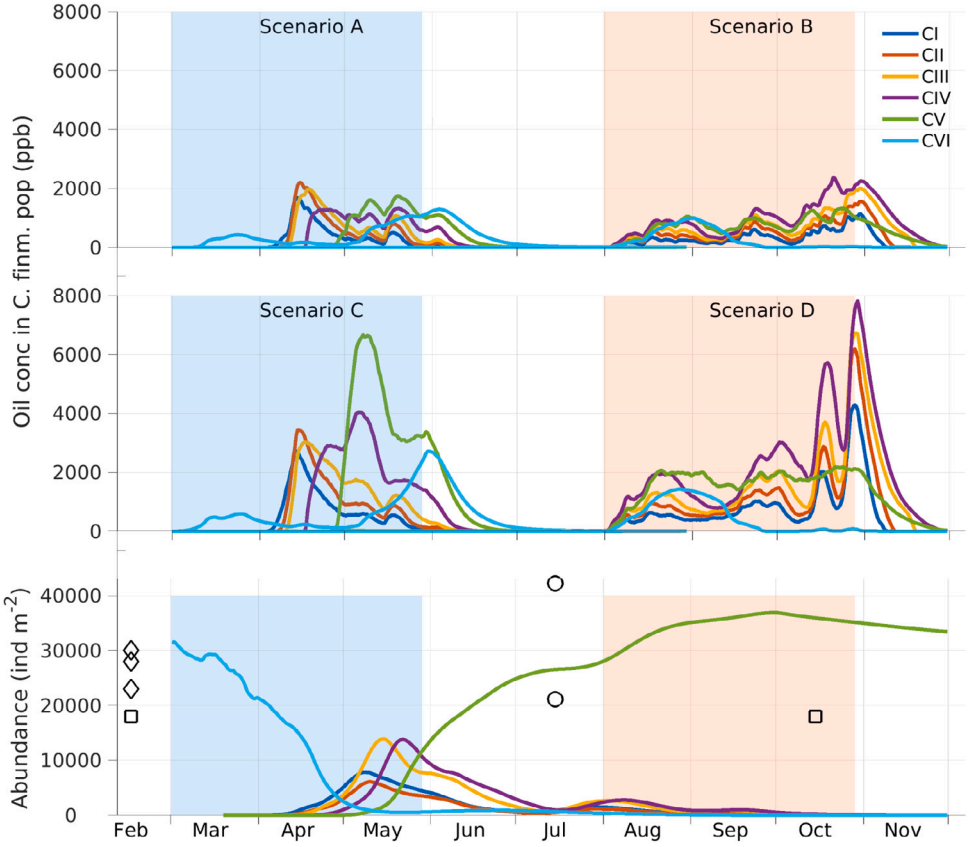

Fig. 10. Time series for the total concentration of oil components (μg (kg wet weight)$^{-1}$) in *C. finmarchicus* stages CI–CVI in scenarios A to D (Table 2). The concentration is calculated as a spatial average over the model subdomain indicated by a yellow rectangle in Fig. 1. The simulated depth integrated average abundances of the CI–CVI stages in the baseline (no oil) scenario are displayed in the bottom panel. The shaded blue and red regions indicate the periods of the March and August oil release, respectively. The symbols (⋄, ∘, □) indicate some observed mean values for *C. finmarchicus* stage CV abundance for the region studied here. The symbols have been placed within the relevant month, but are not from the year (1995) simulated here. ⋄: Halvorsen et al. (2003) (average values for January–February, 2000, 2001, 2002); ∘: Helle (2000) (July 1989, two different regions); □: Melle et al. (2014) (mean values from October to February for the Salten fjord). (For interpretation of the references to color in this figure legend, the reader is referred to the web version of this article.)

Both blowout scenarios led to a much higher average population BB than the surface releases (Fig. 9, bottom). Although there was no direct "local correlation" between TBB_{pop} and external oil concentrations (Fig. 9), on a larger spatial scale the larger volumes of high oil concentrations lead to higher TBB_{pop}s. This is consistent with Fig. 7. In all scenarios the TBB decreased consistently after the oil release stopped.

The stage CV copepods were present in great abundances from June onwards (Fig. 10, bottom panel). Despite a higher lipid content they did not stand out among the CI–CVI stages in terms of TBB (Fig. 10, top and middle panel) in Scenarios B and D (August).

3.4. Lethal and sub lethal effects

On a population scale the effects of the oil release on *C. finmarchicus* in terms of increased mortality and reduced reproduction were minor. Mortality and reproduction reduction (m and $1-r$ in Eqs. (4) and (5)) reached high values near 0.5 d^{-1} (m) and low values near 0.1d^{-1} ($1-r$) for some copepodite stages. Values of m above 10^{-3} occurred in 10% of the instances where $m > 0$, while the median value of the same set was 7×10^{-6} (supplementary figures S1 and S2).

Scenarios C and D (subsea blowouts) resulted in the highest impacts on total mortality and reproduction. The biomass on the shelf around the release point (shelf region within yellow box in Fig. 1) was reduced by a fraction of 10^{-4} to 10^{-3} from the baseline scenario (Fig. 11). The impact of the oil release on the biomass peaked from early May into early June in Scenario C and the end of September in Scenario D (Fig. 11) and then slowly decreased. At the maximum effects, the total biomass was 130 (resp. 160) t carbon lower in Scenario C (resp. D) than in the baseline scenario, corresponding to a wet weight loss of about 1300 (1600) t *C. finmarchicus* (cf. Eq. (3)). Biomass losses due to the oil release were considerably lower in the other scenarios (A, B).

Effects on egg production rates occur at lower TBBs than for mortality (Eqs. (4) and (5), supplementary Figs. S1 and S2). In general, the effects of oil exposure on egg production were low in all scenarios.

4. Discussion

The simulation results described here indicate that there are a number of factors interacting to potentially cause damage to the *C. finmarchicus* population in the case of an oil spill or a subsea blowout. We delve into these next when we discuss the results from each of the results Sections 4.1–4.3 and go into some aspects of match–mismatch between the *C. finmarchicus population* and the dissolved oil 4.4. A final Section 4.5 discusses the ramification and validity of the approach in a greater context.

4.1. Oil spill patterns

In the present case, the energetic blowout conditions generate strong turbulence near the release point. This produces smaller oil droplets which stay submerged and dissolve more rapidly than larger droplets produced from wind-wave induced breakup of a surface oil slick. A recent review provides more detail on the processes governing oil droplet formation, and the modeling of these processes Nissanka and Yapa (2018). In addition, the blowout plume was trapped at around

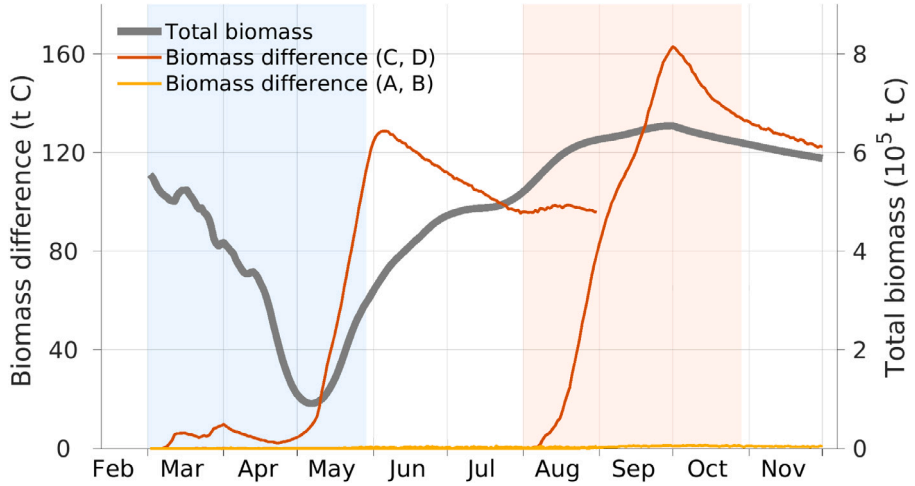

Fig. 11. Time series for the total biomass (gray curve) of *C. finmarchicus* in the shelf part (depth < 500 m) of the yellow box in Fig. 1 in the baseline scenario and the differences in total biomass between the oil release scenarios and the baseline scenarios. The red curves represent the difference in biomass between the scenario without any oil release and Scenarios C and D (red curves; left ordinate axis) over the same region. The yellow curves represent the differences between the scenario without any oil and Scenarios A and B (yellow curves; left ordinate axis) over the same region. The shaded blue and red regions indicate the periods of the March and August oil releases, respectively. (For interpretation of the references to color in this figure legend, the reader is referred to the web version of this article.)

60 m depth, which further promoted submerged droplets (Fig. 7). The surface scenarios displayed variable mixing depths, caused by wind and wave action, with the highest concentrations near the surface, and with low oil concentrations below 50 m. In the blowout scenarios the highest concentrations occurred near the trapping depth (60 m), with mixing both upwards and downwards from this depth, and generally higher concentrations.

4.2. Bioaccumulation

The highest content of oil components in the *C. finmarchicus* population in May (Fig. 9), was due mainly to the retention by stages CIV–CVI (Fig. 10). In Scenarios B and D (August) stages CI–CIV had the highest concentrations while the CV stages dominated the population. The reason for this was that many of these CV copepods had reached, or were reaching, diapause and moved towards the bottom on the shelf (200–300 m depth) and deeper wherever possible, and thus resided below the main oil plume (Fig. 7).

4.3. Lethal and sub lethal effect

Many aquatic organisms experience mortality at TBBs of nonpolar organic compounds at 50 mmol (kg lipid)$^{-1}$ and above (Meador et al., 2011). In the present simulations (Table 1, supplementary figures S1, S2) this corresponds to $m = 6 \times 10^{-3}$. The present (dynamical) model uses mortality *rates* rather than mortality (LC50 values), linked through Eq. (4) (DeLaender et al., 2011). This means that even low TBBs lead to some animals dying. This is justified because the number of individuals within a single model grid cell is very large even at low concentrations, accounting for some natural individual variation in the responses to accumulated oil components.

The effect of the accumulated oil components on the *C. finmarchicus* population (Fig. 11) was diluted after the oil release stopped. This dilution was due to advection of the animals into and out of the shelf part of the yellow region in Fig. 1. In Scenario D (August, subsea blowout), the dilution started before the oil release stopped. This was caused by the gradual descent of the overwintering CV animals under 500 m depth, and also the fact that the mortality for the overwintering CV animals is higher in the relatively shallow waters on the shelf (c.f. the gray curve in Fig. 11).

The main loss in biomass was connected to stage CV animals (Fig. 4) which had the highest TBB ($TBB_{w,V}$) in scenario C and an increase in abundance coinciding with the mortality effect. In the present simulations this can be linked to the relatively high lipid content (and total weight, Fig. 4) of stage CV, with correspondingly higher bioaccumulation than the other stages. The CVI stage also had high TBBs ($TBB_{w,VI}$) at the end of May (Fig. 4), but the number of stage CVI copepodites were few at this time. Thus, a combination of developmental stage, timing of the oil release, place and properties of the animals leads to the simulated large scale effect on the population. The effects were most noticeable after almost three months of oil release in the March scenarios (A, C) (Fig. 11) and after two months in the August scenarios (B, D). CV animals were descending and entering diapause at this time (May–June). The slow "dilution" of the mortality effects in both the March and the August release scenarios are a consequence of the loss of mainly CV animals that are in or entering into diapause, and the limited potential for biological production to compensate for oil related mortality losses during this time of the year.

The cause of the minor effects of the accumulated oil on the egg production was a large fraction of the reproductive females (stage CVI) being advected from the South or onto the shelf and hence were exposed to little or no oil before producing eggs. The $TBB_{w,CVI}$ were relatively low and similar in both Scenarios A and C until the beginning of May (Fig. 10).

4.4. Match–mismatch

We identify three types of match–mismatch between the oil released and the *C. finmarchicus* population related to space, time, and population structure. In some cases, a combination of two or three of these factors operate simultaneously.

A main cause of mismatch is the physical oceanography of the LoVe region. The NAC and the NCC systems represent natural transport barriers along the shelf break. Because of this barrier, animals living off the shelf will be minimally exposed to oil released from an oil discharge point located on the shelf (here defined to be the region with bottom depth < 500 m). However, the barrier effect caused by the interplay of the two current systems is not the only factor that results in the limited oil exposure of *C. finmarchicus* seen from the simulation results (Fig. 8).

In the simulations, the *C. finmarchicus* copepods occupy the water column from 10 to 50 m depth (see also Conover (1988)). In our surface releases (Scenarios A, B; Table 2) the highest oil concentrations occurred in the uppermost layers, mostly above 25 m depth (Scenarios C, D; Fig. 7), but in the subsea blowouts the maximum concentrations

occurred mostly below 50 m depth due to plume trapping. Thus for the subsea releases, copepods were not exposed to the highest water concentrations of oil.

A combination of temporal, spatial and population structure mismatch occurred in the August release scenarios (scenarios B, D). Both the shelf and the deep trenches along the Lofoten–Vesterålen shelf break lie a lot deeper (>200–300 m) than the main oil plume (25 to 100 m) in these scenarios (Fig. 7). By August, a large part of the *C. finmarchicus* population and biomass is in, or is going into, diapause and reside below the oil plume, causing limited exposure for the most abundant stage (CV) and hence less bioaccumulation in this stage than in the March simulations. See also (Broch et al., 2013). However, the August subsea blowout the effect on the *C. finmarchicus* population is still the most severe in terms of the absolute biomass affected (Fig. 11) because the population is dominated by the CV stage at this time. This suggests a potential for even more severe effects with an oil plume positioned at greater depths.

In March and April there was a mismatch between the presence of oil (released off Lofoten/Nordland, Fig. 1) and the main part of the *C. finmarchicus* biomass (consisting of stage VI copepodites) that resides further south at this time (Fig. 2, upper panel). However, by the end of April, the younger calanus developed into the larger, more lipid-rich stage CV and the relation between total *C. finmarchicus* biomass and the TBB_{pop} was almost reciprocal (Figs. 9 , 10). These, more lipid-rich CV calanus are more prone to bioaccumulation (Hendriks et al., 2001).

An additional example of the match–mismatch effect between oil and calanus is observed in the March blowout scenario (scenario C). This scenario is the best example of a match between the presence of oil and calanus on the shelf. Here we observe a (relatively) high mortality in the CV stages. This is relevant because we expect that a high mortality in the CV stages will propagate to an impact on the size of the overwintering population (Fig. 11).

These examples of the interplay of temporal, spatial, and population structure features in determining the effects of oil spills on the population of *C. finmarchicus* in the LoVe region underscore that for Ecosystem Risk Assessment it is essential to have available modeling systems that can address complex, interacting physical and biological features in three dimensional space and time.

4.5. Model validity and uncertainty

Full validation of the simulation results and the model system is infeasible. However, we have assimilated and applied available scientific knowledge to make the model a valid tool to support hypothesis development. The results point towards several interesting phenomena related to the interactions between space, time, and the demographics of the *C. finmarchicus* population. While more specialized models without spatial resolution (“box model”, or 1D models) may be more appropriate in some settings, they will necessarily produce different results from spatial models (DeHoop et al., 2016).

4.5.1. Model resolution

The present simulations applied a coarse horizontal resolution of 4 km, a compromise to allow for longer simulation scenarios and to cover a greater geographical region. Higher spatial resolution provides a more “dynamical" picture of e.g. the *C. finmarchicus* biomass and greater spatial heterogeneity (Broch et al., 2013) due to better resolution of oceanographic features, but at the disadvantage of higher computational cost. Even the fairly large model domain used in the present study seems too small to fully track the oil components in the biota.

4.5.2. Bioaccumulation model OMEGA

The uptake of oil components in the OMEGA model is sensitive to the lipid content of the organism (Hendriks et al., 2001). The lipid content in *C. finmarchicus* is highly variable even within the same stage in the same field sample (Bergvik et al., 2012). The values from (Eq. (2)) correspond well with the total lipid content recorded in Falk-Petersen et al. (2009) (10 –39 μ g ind^{-1} in the model against 20 μg ind^{-1} for stage CIV, 49 –79 against 40 μg ind^{-1} for stage CV, and 66 against 85 μg ind^{-1} for stage CVI), but not so well for the CV content reported in McKinstry et al. (2013) (109–181 μg ind^{-1}). OMEGA is further sensitive to the log Kow of the oil compounds. Since the present model uses pseudocomponents, representing groups of components, this is another source of uncertainty.

4.5.3. Toxicity parameters

De Hoop et al. (2017) found that the calculations of the lethal effects from the TBB of oil components (Eqs. (4), (5)) in fish and crustaceans by the OMEGA model were both over (after short time exposure) and under (after longer time exposure) estimated. The toxicity parameter values used here (Table 1) were based on average species sensitivities (DeHoop et al., 2016). Some of the results presented in DeHoop et al. (2016) were based on the SYMBIOSES model system with a slightly different oil release point and different oil composition than the ones used here. More severe ($LBB = 12.3$, $\gamma = 5.36$, $q_{\mathrm{ls}} = 1.06$, and $T_{\mathrm{exp}} = 10$ in Eq. (4)) toxicity parameters manifested themselves in higher mortality and lower *C. finmarchicus* biomass than by using the present parameters. The effects of increasing the toxicity of the oil components were severe (up to a 80% lower biomass than the baseline) in a single model grid cell close by the release point (for the year 2001). The average reduction in biomass from the baseline over a greater region (~100 × 100 km) was at most about 5%. A simulation study with a higher resolution (800 m) model domain covering approximately the region considered in the present paper (yellow box in Fig. 1) revealed that “killing" *all C. finmarchicus* within one model grid cell (an extreme worst-case acute effects scenario) led to a simulated decrease in biomass in that region by 0–1% (Broch et al., 2013).

In all the simulations the mortality effects were diluted with time as the oil release stopped and new animals were advected into the region.

4.5.4. Consequences for starvation of cod larvae and other fish species

The reduction in spawning due to the accumulated oil components did not, on average, significantly reduce the number of eggs and nauplii. While cod larvae initially feed mainly on nauplii of copeods, large phytoplankton may also be included in the diet, and later stages feed on zooplankton copepodites; see Ottersen et al. (2014) and references therein. Thus, the impact of the oil accumulation in *C. finmarchicus* on the survival of cod larvae would have been minor. Similarly, for other species feeding on either *C. finmarchicus* nauplii or copepodites, the effects on survival would have been minor, as the maximum reduction in *C. finmarchicus* biomass in Scenario C over the selected area (yellow box in Fig. 1) was 0.05%. Due to the coarse model resolution, very local effects could have been more severe. Effects were over all less noticeable in spring than in summer.

4.5.5. Trophic transfer of oil components

Trophic transfer to or from *C. finmarchicus* were not taken into account in the present simulations. Combined laboratory and kinetic modeling experiments have indicated that dietary exposure to dissolved oil components through phytoplankton may be as important as aqueous exposure for *Acartia erythraea* (Wang and Wang, 2006), but little information on *Calanus* is available for oil components. Oil component bioaccumulation may have detrimental effects on the phytoplankton, depending on the species (Bretherton et al., 2018). The presence of phytoplankton and protozoa following an oil spill may however reduce the potential for PAH bioaccumulation in zooplankton. Protozoa may egest oil components that are subsequently excreted in

fecal pellets (Almeda et al., 2014), thus contributing to the formation of marine snow (Brakstad et al., 2018) and to vertical export of the oil components.

Herring fed a *C. finmarchicus* diet containing up to 9×10^5 μg crude oil kg WW^{-1} (9 times the high end of the scale in Fig. 8) showed signs of sublethal (transcriptional) effects after 2 months' exposure time (Olsvik et al., 2011). Such concentrations for a similar time period seem to be unrealistic in the present scenarios.

4.5.6. Transfer of oil components to offspring, diapause, and long term effects

Transfer of bioaccumulated oil components to eggs has not been considered. There are indications that this has a minor long term effect on the nauplii (Hansen et al., 2017), with a potential for further transfer to, *e.g.*, cod larvae. Long term effects of oil exposure to copepodites during diapause through winter may lead to decreased survival, reduced egg production in *C. glacialis* (Toxværd et al., 2018), and delayed surface migration in *C. finmarchicus* (Skottene et al., 2019). In the present simulations, the mortality effect is taken into account, but the long term sublethal effects are not. Although there is a clear indication of bioaccumulation of oil components, the present results indicate that a surface oil spill or a subsea blowout on the shelf may have a minor impact only due to limited vertical overlap between the dissolved oil components and the diapausing CV stage.

5. Conclusions

We found differences in the bioaccumulation of oil components in *Calanus finmarchicus* to oil spills occurring in the Lofoten–Vesterålen archipelago with discharge type (surface or subsea blowout) and time of spill occurrence (spring, late summer). Differences were related to the varying degrees of overlap between oil and *C. finmarchicus* in space and time. With respect to time of release, bioaccumulation was lowest for the late summer scenarios. At this time much of the adult population has already descended to deeper along the shelf break making them less likely to encounter oil released from a spill. With respect to discharge type, blowout scenarios led to higher average body burdens for the population compared to surface scenarios. In blowouts, turbulence at the release point leads to smaller oil droplets which stay submerged and dissolve more rapidly than droplets produced from wind-wave induced breakup of a surface oil slick. The highest bioaccumulation of oil components in the zooplankton occurred for the blowout scenario in spring.

Because the NCC and NAC are partially functioning as transport barriers along the outer part of the Lofoten–Vesterålen archipelago, the exchange of oil off the shelf region is limited. As a result, there was minimal bioaccumulation of oil components in zooplankton found in waters beyond the shelf region. For all combinations of discharge type and time of spill occurrence, the effects of oil on egg production and mortality on *C. finmarchicus* populations were minor, but with a greater impact in the subsea blowout scenarios than in the surface release scenarios. Combinations of match/mismatch mechanisms involving spatial, temporal and population structure features of the zooplankton population tend to limit the overlap of oil and *C. finmarchicus* in the environment. And as a result, effects at the population level are minor. While acute and short-term effects were found to be small, we cannot rule out the potential for more significant long term, chronic effects. Further knowledge combined with modeling investigations will be needed to address how the population responds to long term, chronic effects.

CRediT authorship contribution statement

Ole Jacob Broch: Conceptualization, Methodology, Software, Formal analysis, Investigation, Writing - original draft, Writing - review & editing, Visualization. **Raymond Nepstad:** Conceptualization, Methodology, Software, Formal analysis, Investigation, Writing - original draft, Writing - review & editing, Visualization. **Ingrid Ellingsen:** Methodology, Software, Writing - original draft, Writing - review & editing, Visualization. **Radovan Bast:** Methodology, Software, Resources, Data curation, Writing - review & editing. **Geir Morten Skeie:** Methodology, Software, Resources, Data curation, Writing - review & editing. **JoLynn Carroll:** Conceptualization, Investigation, Writing - original draft, Writing - review & editing, Project Administration, Funding acquisition.

Declaration of competing interest

The authors declare that they have no known competing financial interests or personal relationships that could have appeared to influence the work reported in this paper.

Acknowledgments

The following persons provided knowledge in support of the development of the model system: Frode Vikebø, Daniel Howell, Starrlight Augustine, Jonas Juselius, Morten Omholt Alver, Martin Biuw, Bjarte Bogstad, Katrin Bluhm, Ute Brönner, Raoul-Marie Couture, Frederik de Laender, Lisette de Hoop, Bjørn Einar Grøsvik, A. Jan Hendriks, Chris Klok, Øystein Langangen, Jannicke Moe, Mark Reed, Dag Slagstad, Petter Rønningen, Karel Viaene, Magnus Wiedmann, and Lindsay Wilson. The simulations were performed on resources provided by UNINETT Sigma2 — the National Infrastructure for High Performance Computing and Data Storage in Norway (NN9295K). Financial support for this project was provided by the Research Council of Norway (RCN) (projects 208300/E30, 203823/E40, 235150/E30, 243047, and 228107). Some of these RCN grant programs are contingent upon additional financial contributions from industry. The following companies provided additional financial contributions: Equinor Energy, ConocoPhillips Skandinavia, DEA Norge, Vår Energi, OMV, Lundin, Aker BP, ExxonMobil Upstream Research Company, Shell Norway and Total E & P Norway. The findings presented in this manuscript are those of the coauthors and associated researchers listed in acknowledgments. Industry investors received no censorship rights in the analysis, interpretation, or reporting of our research results.

Bjørn Henrik Hansen (SINTEF) provided useful information on toxic effects of oil in the marine environment. The three anonymous referees provided feedback that improved the paper significantly.

Appendix A. Supplementary data

Supplementary material related to this article can be found online at https://doi.org/10.1016/j.marenvres.2020.105184.

References

Almeda, R., Connelly, T.L., Buskey, E.J., 2014. Novel insight into the role of heterotrophic dinoflagellates in the fate of crude oil in the sea. Sci. Rep. 4, 7560.

Alver, M.O., Broch, O.J., Melle, W., Bagøien, E., Slagstad, D., 2016. Validation of an Eulerian population model for the marine copepod *Calanus finmarchicus* in the Norwegian Sea. J. Mar. Syst. 160, 81–93.

Anon, 2011. LOfoten and VEsterålen CURrents (LOVECUR). Comparison of Hindcasts with Measurements. Revision 2. Technical Report, Forristall Ocean Engineering, Inc.

Bergvik, M., Leiknes, Ø., Altin, D., Dahl, K.R., Olsen, Y., 2012. Dynamics of the lipid content and biomass of *Calanus finmarchicus* (copepodite V) in a Norwegian fjord. Lipids 47 (9), 881–895. http://dx.doi.org/10.1007/s11745-012-3700-3.

Brakstad, O.G., Lewis, A., Beegle-Krause, C., 2018. A critical review of marine snow in the context of oil spills and oil spill dispersant treatment with focus on the Deepwater Horizon oil spill. Mar. Pollut. Bull. (ISSN: 0025-326X) 135, 346–356. http://dx.doi.org/10.1016/j.marpolbul.2018.07.028, URL http://www.sciencedirect.com/science/article/pii/S0025326X1830506X.

Bretherton, L., Williams, A., Genzer, J., Hillhouse, J., Kamalanathan, M., Finkel, Z.V., Quigg, A., 2018. Physiological response of 10 phytoplankton species exposed to Macondo oil and the dispersant, Corexit. J. Phycol. 54 (3), 317–328. http://dx.doi.org/10.1111/jpy.12625.

Broch, O.J., Slagstad, D., Smit, M., 2013. Modelling produced water dispersion and its direct toxic effects on the production and biomass of the marine copepod *Calanus finmarchicus*. Mar. Environ. Res. (ISSN: 0141-1136) 84, 84–95. http://dx.doi.org/10.1016/j.marenvres.2012.12.003, URL http://www.sciencedirect.com/science/article/pii/S0141113612002218.

Carlotti, F., Krause, M., Radach, G., 1993. Growth and development of calanus finmarchicus related to the influence of temperature: Experimental results and conceptual model. Limnol. Oceanogr. 38 (6), 1125–1134. http://dx.doi.org/10.4319/lo.1993.38.6.1125.

Carroll, J., Vikebø, F., Howell, D., Broch, O.J., Nepstad, R., Augustine, S., Skeie, G.M., Bast, R., Juselius, J., 2018. Assessing impacts of simulated oil spills on the Northeast Arctic cod fishery. Mar. Polut. Bull. 126, 63–73.

Conover, R.J., 1988. Comparative life histories in genera *Calanus* and *Neocalanus* in high latitudes of the northern hemisphere. Hydrobiologia 167/168, 127–142.

Coyle, K.O., Gibson, G.A., 2017. *Calannus* on the bering sea shelf: probably cause for populations declines during warm years. J. Plankton Res. 39, 257–270.

De Hoop, L., Viaene, K.P., Schipper, A.M., Huijbregts, M.A., De Laender, F., Hendriks, A.J., 2017. Time-varying effects of aromatic oil constituents on the survival of aquatic species: Deviations between model estimates and observations. Environ. Toxicol. Chem. 36 (1), 128–136. http://dx.doi.org/10.1002/etc.3508.

Dee, D.P., Uppala, S.M., Simmons, A.J., Berrisford, P., Poli, P., Kobayashi, S., Andrae, U., Balmaseda, M.A., Balsamo, G., Bauer, P., Bechtold, P., Beljaars, A.C.M., van de Berg, L., Bidlot, J., Bormann, N., Delsol, C., Dragani, R., Fuentes, M., Geer, A.J., Haimberger, L., Healy, S.B., Hersbach, H., Hólm, E.V., Isaksen, L., Kållberg, P., Köhler, M., Matricardi, M., McNally, A.P., Monge-Sanz, B.M., Morcrette, J.-J., Park, B.-K., Peubey, C., de Rosnay, P., Tavolato, C., Thépaut, J.-N., Vitart, F., 2011. The ERA-interim reanalysis: configuration and performance of the data assimilation system. Q. J. R. Meteorol. Soc. 137 (656), 553–597. http://dx.doi.org/10.1002/qj.828.

DeHoop, L., Broch, O., Hendriks, A.J., Laender, F.D., 2016. Crude oil affecting the biomass of the marine copepod *Calanus finmarchicus*: Comparing a simple and complex population model. Mar. Environ. Res. 119, 197–206.

DeLaender, F., Olsen, G.H., Frost, T., Grøsvik, B.E., Grung, M., Hansen, B.H., Hendriks, A.J., Hjorth, M., Janssen, C.R., Klok, C., Nordtug, T., Smit, M., Carroll, J., Camus, L., 2011. Ecotoxicological mechanisms and models in an impact analysis tool for oil spills. J. Toxicol. Environ. Health A 74 (7–9), 605–619, PMID: 21391101. https://doi.org/10.1080/15287394.2011.550567.

Falk-Petersen, S., Mayzaud, P., Kattner, G., Sargent, J.R., 2009. Lipids and life strategy of Arctic *Calanus*. Mar. Biol. Res. 5, 18–39.

Gascard, J.-C., Raisbeck, G., Sequeira, S., Yiou, F., Mork, K.A., 2004. The Norwegian Atlantic Current in the Lofoten basin inferred from hydrological and tracer data (129I) and its interaction with the Norwegian Coastal Current. Geophys. Res. Lett. 31 (1), http://dx.doi.org/10.1029/2003GL018303.

Halvorsen, E., Tande, K.S., Edvardsen, A., Slagstad, D., Pedersen, O.P., 2003. Habitat selection of overwintering *Calanus finmarchicus* in the NE Norwegian Sea and shelf waters off Northern Norway in 2000-2. Fish. Oceanogr. 12, 339–351.

Hansen, B.H., Tarrant, A.M., Salaberria, I., Altin, D., Nordtug, T., Øverjordet, I.B., 2017. Maternal polycyclic aromatic hydrocarbon (PAH) transfer and effects on offspring of copepods exposed to dispersed oil with and without oil droplets. J. Toxicol. Environ. Health A 80 (16–18), 881–894, PMID: 28841382. https://doi.org/10.1080/15287394.2017.1352190.

Helaouët, P., Beaugrand, G., 2009. Physiology, ecological niches and species distribution. Ecosystems 12 (8), 1235–1245.

Helle, K., 2000. Distribution of the copepodite stages of *Calanus finmarchicus* from Lofoten to the Barents Sea in July 1989. ICES J. Mar. Sci. 57, 1636–1644.

Hendriks, A.J., van der Linde, A., Cornelissen, G., Sijm, D.T.H.M., 2001. The power of size. 1. Rate constants and equilibrium ratios for accumulation of organic substances related to octanol-water partition ratio and species weight. Environ. Toxicol. Chem. 20 (7), 1399–1420. http://dx.doi.org/10.1002/etc.5620200703.

Howell, D., Bogstad, B., 2010. A combined Gadget/FLR model for management strategy evaluations of the Barents Sea fisheries. ICES J. Mar. Sci. 67, 1998–2004.

Isachsen, P.E., 2015. Baroclinic instability and the mesoscale eddy field around the Lofoten Basin. J. Geophys. Res.: Oceans 120 (4), 2884–2903. http://dx.doi.org/10.1002/2014JC010448.

Johansen, Ø., 2000. Deepblow – a Lagrangian plume model for deep water blowouts. Spill Sci. Technol. Bull. 6 (2), 103–111.

Jónasdóttir, S.H., Visser, A.W., Richardson, K., Heath, M.R., 2015. Seasonal copepod lipid pump promotes carbon sequestration in the deep North Atlantic. Proc. Natl. Acad. Sci. 112 (39), 12122–12126.

Lee, Y.J., Matrai, P.A., Friedrichs, M.A.M., Saba, V.S., Aumont, O., Babin, M., Buitenhuis, E.T., Chevallier, M., de Mora, L., Dessert, M., Dunne, J.P., Ellingsen, I.H., Feldman, D., Frouin, R., Gehlen, M., Gorgues, T., Ilyina, T., Jin, M., John, J.G., Lawrence, J., Manizza, M., Menkes, C.E., Perruche, C., Le Fouest, V., Popova, E.E., Romanou, A., Samuelsen, A., Schwinger, J., Séférian, R., Stock, C.A., Tjiputra, J., Tremblay, L.B., Ueyoshi, K., Vichi, M., Yool, A., Zhang, J., 2016. Net primary productivity estimates and environmental variables in the arctic ocean: An assessment of coupled physical-biogeochemical models. J. Geophys. Res.: Oceans 121 (12), 8635–8669. http://dx.doi.org/10.1002/2016JC011993.

McKinstry, C.A.E., Westgage, A.J., Koopman, H.N., 2013. Annual variation in the nutritional value of Stage V *Calanus finmarchicus*: implications for right whales and other copepod predators. Endang. Species Res. 20, 195–204.

Meador, J.P., Adams, W.J., Escher, B.I., McCarty, L.S., McElrou, A.E., Sappington, K.G., 2011. The tissue residue approach for toxicity assessment: Finding and critical review from a society of environmental toxicology and chemistry pellston workshop. Integr. Environ. Assess. Manage. 7, 2–6.

Melle, W., Runge, J., Head, E., Plourde, S., Castellani, C., Licandro, P., Pierson, J., Jonasdottir, S., Johnson, C., Broms, C., Debes, H., Falkenhaug, T., Gaard, E., Gislason, A., Heath, M., Niehoff, B., Nielsen, T.G., Pepin, P., Stenevik, E.K., Chust, G., 2014. The North Atlantic Ocean as habitat for *Calanus finmarchicus*: Environmental factors and life history traits. Prog. Oceanogr. (ISSN: 0079-6611) 129, 244–284, North Atlantic Ecosystems, the role of climate and anthropogenic forcing on their structure and function. http://dx.doi.org/10.1016/j.pocean.2014.04.026. URL http://www.sciencedirect.com/science/article/pii/S0079661114000743.

Misund, O.A., Olsen, E., 2013. Lofoten-vesterålen: for cod and cod fisheris, but not for oil? ICES J. Mar. Sci 70, 722–725.

Mitchelson-Jacob, G., Sundby, S., 2001. Eddies of Vestfjorden, Norway. Cont. Shelf Res. (ISSN: 0278-4343) 21 (16), 1901–1918. http://dx.doi.org/10.1016/S0278-4343(01)00030-9, URL http://www.sciencedirect.com/science/article/pii/S0278434301000309.

Nissanka, I.D., Yapa, P.D., 2018. Calculation of oil droplet size distribution in ocean oil spills: A review. Mar. Pollut. Bull. 135, 723–734.

Olsvik, P.A., Waagbø, R., Pedersen, S.A., Meier, S., 2011. Transcriptional effects of dietary exposure of oil-contaminated *Calanus finmarchicus* in Atlantic herring (*Clupea harengus*). J. Toxicol. Environ. Health A 74 (7–9), 508–528, PMID: 21391095. https://doi.org/10.1080/15287394.2011.550560.

Ottersen, G., Bogstad, B., Yaragina, N.A., Stige, L.C., Vikebø, F.B., Dalpadado, P., 2014. A reveiw of early life history dynamics of Barents Sea cod (*Gadus morhua*). ICES J. Mar. Sci. 71, 2064–2087.

Pan, Q., Yu, H., Daling, P.S., Zhang, Y., Reed, M., Wang, Z., Li, Y., Wang, X., Wu, L., Zhang, Z., Yu, H., Zou, Y., 2020. Fate and behavior of Sanchi oil spill transported by the Kuroshio during January–February 2018. Mar. Pollut. Bull. (ISSN: 0025-326X) 152, 110917. http://dx.doi.org/10.1016/j.marpolbul.2020.110917, URL http://www.sciencedirect.com/science/article/pii/S0025326X20300357.

Reed, M., Daling, P.S., Brakstad, O.G., Singsaas, I., Faksness, L.-G., Hetland, B., Ekrol, N., 2000. OSCAR2000: a multi-component 3-dimensional Oil Spill Contingency and Response model. In: Arctic and Marine Oilspill Program Technical Seminar. Environment Canada; 1999, pp. 663–680.

Reed, M., Daling, P., Lewis, A., Ditlevsen, M.K., Brørs, B., Clark, J., Aurand, D., 2004. Modelling of dispersant application to oil spills in shallow coastal waters. Environ. Model. Softw. 19 (7), 681–690.

Rye, H., Reed, M., Frost, T.K., Smit, M.G.D., Durgut, I., Johansen, Ø., Ditlevsen, M.K., 2008. Development of a numerical model for calculating exposure to toxic and nontoxic stressors in the water column and sediment from drilling discharges. Integr. Environ. Assess. Manage. 4 (2), 194–203.

Sætre, R. (Ed.), 2007. The Norwegian Coastal Current. Tapir Academic Press.

Skardhamar, J., Svendsen, H., 2005. Circulation and shelf-ocean interactions off North Norway. Cont. Shelf. Res. 25, 1541–1560.

Skottene, E., Tarrant, A.M., Olsen, A.J., Altin, D., Hansen, B.H., Choquet, M., Olsen, R.E., Jenssen, B.M., 2019. A crude awakening: Effects of crude oil on lipid metabolism in calanoid copepods terminating diapause. Biol. Bull. 237 (2), 90–110, PMID: 31714858. https://doi.org/10.1086/705234.

Slagstad, D., 1981. Modeling and simulation of phyisology and population dynamics of copepods. Effects of physical and biological parameters. Model. Identif. Control 2, 119–162.

Slagstad, D., McClimans, T.A., 2005. Modelling the ecosystem dynamics of the Barents sea including the marginal ice zone: I. Physical and chemical oceanography. J. Mar. Syst. 58, 1–18.

Slagstad, D., Tande, K.S., 2007. Structure and resilience of overwintering habitats of *Calanus finmarchicus* in the Eastern Norwegian Sea. Deep Sea Res. II (ISSN: 0967-0645) 54 (23), 2702–2715, Effects of Climate Variability on Sub-Arctic Marine Ecosystems. http://dx.doi.org/10.1016/j.dsr2.2007.08.024. URL http://www.sciencedirect.com/science/article/pii/S0967064507002093.

Slagstad, D., Tande, K.S., Wassman, P., 1999. Modelled carbon fluxes as validated by field dta on the north Norwegian shelf during the productive period in 1994. Sarsia 84 (3–4), 303–317. http://dx.doi.org/10.1080/00364827.1999.10420434.

Toxværd, K., Van Dinh, K., Henriksen, O., Hjorth, M., Nielsen, T.G., 2018. Impact of pyrene exposure during overwintering of the Arctic copepod *Calanus glacialis*. Environ. Sci. Technol. 52 (18), 10328–10336, PMID: 30130096. https://doi.org/10.1021/acs.est.8b03327.

Vernet, M., Ellingsen, I.H., Seuthe, L., Slagstad, D., Cape, M.R., Matrai, P.A., 2019. Influence of phytoplankton advection on the productivity along the Atlantic water inflow to the Arctic Ocean. Front. Mar. Sci. (ISSN: 2296-7745) 6, 583, URL https://www.frontiersin.org/article/10.3389/fmars.2019.00583.

Wang, X., Wang, W.-X., 2006. Bioaccumulation and transfer of benzo(a)pyrene in a simplified marine food chain. Mar. Ecol. Prog. Ser. 312, 101–111.

Wassmann, P., Slagstad, D., Ellingsen, I., 2019. Advection of mesozooplankton into the Northern Svalbard Shelf region. Front. Mar. Sci. (ISSN: 2296-7745) 6, 458, URL https://www.frontiersin.org/article/10.3389/fmars.2019.00458.

Wassmann, P., Slagstad, D., Riser, C.W., Reigstad, M., 2006. Modelling the ecosystem dynamics of the Barents Sea including the marginal ice zone II. Carbon flux and interannual variability. J. Mar. Syst. 59, 1–24.

Weidberg, N., Basedow, S.L., 2019. Long-term variability in overwintering copepod populations in the Lofoten Basin: The role of the North Atlantic oscillation and trophic effects. Limnol. Oceanogr. 64 (5), 2044–2058. http://dx.doi.org/10.1002/lno.11168.